Probing quark transverse momentum distributions in the color glass condensate: Quark-gluon dijets in deep inelastic scattering at next-to-eikonal accuracy

Tolga Altinoluk[ORCID]

Theoretical Physics Division, National Centre for Nuclear Research, Pasteura 7, Warsaw 02-093, Poland

Néstor Armesto[ORCID]

*Departamento de Física de Partículas and IGFAE, Universidade de Santiago de Compostela,
15782 Santiago de Compostela, Galicia, Spain*

Guillaume Beuf[ORCID]

Theoretical Physics Division, National Centre for Nuclear Research, Pasteura 7, Warsaw 02-093, Poland

We study the production, in deep inelastic scattering at high energy, of a quark-gluon dijet induced by t-channel quark exchange with the target, which goes beyond the eikonal approximation. Throughout this study we follow the color glass condensate approach, keep full dependence on the quark mass and consider the target to be unpolarized. We focus on the correlation limit in which the produced jets fly almost back-to-back and find a factorized expression for the cross section, for both longitudinal and transverse photons, involving the unpolarized quark transverse momentum dependent distribution. Quark-gluon dijets can be distinguished from other types of dijets at least in the heavy quark case, thanks to heavy flavor tagging. In that case, the dominant background is expected to come from the eikonal production of a quark-antiquark-gluon system. We propose experimental cuts to suppress that background contribution, making the process of quark-gluon dijet production in deep inelastic scattering a new method to probe the quark transverse momentum dependent distribution at the Electron Ion Collider.

I. INTRODUCTION

Understanding the high-energy behavior of quantum chromodynamics (QCD) is one of the key missing aspects in our knowledge of the strong interaction. Such understanding, intrinsically linked with that of the structure of hadrons in the region where their partons carry a small fraction x of the hadron momentum, is essential for precise predictions of the production of Standard Model (SM) particles at hadronic colliders. Besides, QCD processes are the largest background in the determination of SM parameters and searches for physics beyond the SM.

On general grounds, it is expected that at high energies QCD enters a regime where the linear approximation to QCD radiation breaks and nonlinear effects dominate [1]. Such nonlinear effects, leading to the saturation of parton densities, are enhanced at small values of x and for nuclei.

The color glass condensate (CGC) effective field theory [2] offers a weak coupling but nonperturbative realization of parton saturation.

In recent years it has been realized that the objects describing hadrons in CGC calculations (namely, ensembles of Wilson lines averaged over the color configurations of the hadron) can be related, considering a certain kinematic situation called correlation limit, to the parton distributions discussed in the frame of transverse momentum dependent (TMD) factorization [3,4]. Such relation for dijet [5–9] and trijet [10–12] production have been established for the gluon TMD parton distribution functions at leading order (LO) in the coupling constant at leading twist.[1] Recently, this relation is studied at next-to-leading order (NLO) [15,16] and also at LO but beyond the kinematic leading twist approximation [17–24] for dijet production.

On the other hand, in CGC calculations and, in general, in high-energy QCD the eikonal approximation is used,

---

[1]The sea quark contribution to the quark TMD stemming from gluon splitting was also studied within the CGC in the eikonal limit [13,14].

which results in discarding terms subleading in energy. In recent years, there have been a lot of efforts to go beyond the eikonal approximation and account for the subeikonal contributions [25–58] in various processes. It has been shown that in some observables, such as the ones sensitive to spin, see, e.g., [47], the terms subleading in energy dominate the cross section. Computations at subeikonal accuracy require the consideration of quarks, and not only gluons, exchanged in the t-channel (see, e.g., [35,49]).

The study of hadron and nuclear three-dimensional structure and the search for the nonlinear regime of QCD are, together with the understanding of nucleon spin, the physics pillars of the Electron Ion Collider (EIC) [59,60]. The very large luminosity, together with modern large acceptance detectors, offer unprecedented opportunities for QCD studies. The center-of-mass energy $\sqrt{s_{NN}} \simeq 40$–140 GeV/nucleon, similar to those at the Relativistic Heavy Ion Collider at BNL and lower than at the Large Hadron Collider at CERN or the Hadron-Electron Ring Accelerator at DESY, together with the spin program, require a careful consideration of subeikonal effects.

In this context, here we establish for the first time the relation at small x between CGC and TMD calculations including quark t-channel exchanges that are subdominant in energy and thus can be considered subeikonal. We examine a process determined by the t-channel exchange of a quark: the LO production of a quark-gluon dijet in deep inelastic scattering (DIS) on an unpolarized target. We first compute the scattering amplitudes for transverse and longitudinal virtual photons within the CGC framework. Calculations are done keeping the quark mass. We then go to the correlation limit and compute the cross section. In this limit, the CGC average of the Wilson lines obtained for this process, characterizing the target, can be related to the quark TMD distribution in the hadron target at small x. The cross section shows explicit suppression with the energy compared to gluon exchange. Finally, we discuss how to disentangle this mechanism for qg dijet production from the contributions that do not involve quark TMD distributions.

II. SCATTERING AMPLITUDES FOR QUARK-GLUON DIJET PRODUCTION AT NEXT-TO-EIKONAL ACCURACY IN DIS

With the previously mentioned motivation, we are interested in studying the production of a quark and a gluon (to be interpreted as separate jets) from the interaction of a virtual photon with a nucleus target. More precisely, we focus on the contribution from a single t-channel quark exchange at the amplitude level which is subeikonal. But we resum multiple interactions with the gluon background field. The two relevant diagrams in this case correspond to two different orderings between the photon and radiated gluon vertices along the quark line as

shown on Fig. 1. At high scattering energies, due to the large boost of the target, the quark background field is effectively localized in a parametrically small support along the x^+ direction. This forces one of the two vertices to be inside the small support of the target. By contrast, the other vertex has to be outside of the target in order to avoid further power suppression at high energy. The leading power contributions are shown in Fig. 1. In the first one (called *before* contribution), the photon splits into quark-antiquark before the target like in the standard dipole picture of DIS [61] and then the antiquark is converted to a gluon via interaction with the t-channel quark. In the second one (called *in* contribution), the photon is converted to a quark which then radiates a gluon after exiting the target. At S-matrix level, these two contributions can be written as[2]

$$
\begin{aligned}
S_{\gamma \to q_1 g_2}^{\text{bef}} = \lim_{x^+, y^+ \to +\infty} & \int_{\mathbf{x}, \mathbf{y}} \int_{x^-, y^-} e^{ip_1 \cdot x} \bar{u}(1) \gamma^+ e^{ip_2 \cdot y} \varepsilon_\nu^{\lambda_2}(p_2)^* \\
& \times (-2p_2^+) \int_{w, z} e^{-iq \cdot w} \varepsilon_\mu^\lambda(q) G_F^{\nu\rho}(y, z)_{a_2 b} S_F(x, w) \\
& \times (-iee_f) \gamma^\mu S_F(w, z)(-ig)\gamma_\rho t^b \Psi(z),
\end{aligned}
\tag{1}
$$

$$
\begin{aligned}
S_{\gamma \to q_1 g_2}^{\text{in}} = \lim_{x^+, y^+ \to +\infty} & \int_{\mathbf{x}, \mathbf{y}} \int_{x^-, y^-} e^{ip_1 \cdot x} \bar{u}(1) \gamma^+ e^{ip_2 \cdot y} \varepsilon_\nu^{\lambda_2}(p_2)^* \\
& \times (-2p_2^+) \int_{w, z} e^{-iq \cdot z} \varepsilon_\mu^\lambda(q) G_{F,0}^{\nu\rho}(y, w)_{a_2 b} S_{F,0}(x, w) \\
& \times (-ig)\gamma_\rho t^b S_F(z, w)(-iee_f)\gamma^\mu \Psi(z),
\end{aligned}
\tag{2}
$$

for arbitrary polarization λ of the photon. Here, $\Psi(z)$ is the quark background field, S_F and G_F are the Feynman quark and gluon propagators in the gluon background field of the target at eikonal accuracy, whereas $S_{F,0}$ and $G_{F,0}$ are the corresponding vacuum propagators. The scattering amplitude is defined from the S-matrix element as follows:

$$
S_{\gamma_{T,L} \to q_1 g_2} = (2q^+) 2\pi \delta(p_1^+ + p_2^+ - q^+) i\mathcal{M}_{\gamma_{T,L} \to q_1 g_2}.
\tag{3}
$$

In order to define the power counting associated with the eikonal approximation and to classify subeikonal corrections, we follow the approach from Refs. [32–34], based on scaling properties under a large boost of the target along x^-. In particular, components of vector and tensor quantities associated only with the target have simple scaling properties in light-cone coordinates, determined by their number of upper and lower $+$ and $-$ indices. In the case of a current

---

[2]Throughout this paper, we use the light cone basis for momenta $p = (p^+, p^-, \mathbf{p})$ with $p^\pm = (p^0 \pm p^3)/\sqrt{2}$. Moreover, in what follows m is the quark mass and $Q^2 = -q^2$ is the photon virtuality, and subindices in integrals denote integration variables, i.e., $\int_x = \int dx$, $\int_{\mathbf{x}} = \int d^2\mathbf{x}$.
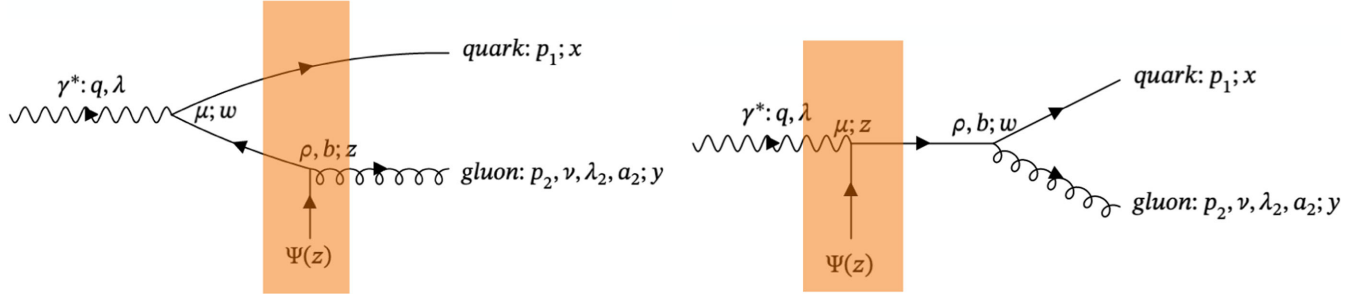
FIG. 1.   Diagrams with photon splitting before (left) or interacting inside (right) the target. Momenta, color, and polarization indices, and coordinates separated by a semicolon, are indicated. The target hadron is shown as an orange band.

associated with the target (for example a color, or flavor or baryon number current), the components should scale as

$$J^-(z) \propto \gamma_t, \qquad J^j(z) \propto (\gamma_t)^0, \qquad J^+(z) \propto (\gamma_t)^{-1}, \qquad (4)$$

under a large boost of the target along the x^- direction, with boost factor γ_t.

In order to setup our calculation, we also need to specify the scaling behavior of the quark background field $\Psi(z)$ of the target. It is convenient to introduce the projections

$$\Psi^{(-)}(z) \equiv \frac{\gamma^+\gamma^-}{2}\Psi(z),$$

$$\Psi^{(+)}(z) \equiv \frac{\gamma^-\gamma^+}{2}\Psi(z), \qquad (5)$$

respectively, on the so-called good (or partonic) components of $\Psi(z)$ of the target and on the bad (or nonpartonic) components of $\Psi(z)$ of the target. Then, currents constructed as bilinears of $\Psi(z)$ have components depending on these two types of components as

$$\bar{\Psi}(z)\gamma^-\Psi(z) = \overline{\Psi^{(-)}}(z)\gamma^-\Psi^{(-)}(z),$$

$$\overline{\Psi}(z)\gamma^j\Psi(z) = \overline{\Psi^{(-)}}(z)\gamma^j\Psi^{(+)}(z) + \overline{\Psi^{(+)}}(z)\gamma^j\Psi^{(-)}(z),$$

$$\overline{\Psi}(z)\gamma^+\Psi(z) = \overline{\Psi^{(+)}}(z)\gamma^-\Psi^{(+)}(z). \qquad (6)$$

Such currents associated with the target have to follow the scaling behavior (4), so that the components of the quark background field scale as

$$\Psi^{(-)}(z) \propto (\gamma_t)^{\frac{1}{2}},$$

$$\Psi^{(+)}(z) \propto (\gamma_t)^{-\frac{1}{2}}, \qquad (7)$$

under a large boost of the target. In our calculation at next-to-eikonal (NEik) accuracy, only the components $\Psi^{(-)}(z)$ matter in Eqs. (1) and (2), whereas the components $\Psi^{(+)}(z)$ would contribute only to corrections which are further suppressed at high energy (next-to-next-to-eikonal (NNEik) and beyond).

Therefore, at S-matrix level, both contributions (1) and (2) have an overall scaling as $(\gamma_t)^{-\frac{1}{2}}$ under a large boost of the

target along the x^- direction, resulting from the enhancement as $(\gamma_t)^{\frac{1}{2}}$ of $\Psi^{(-)}(z)$ and from the suppression as $(\gamma_t)^{-1}$ due to the integration in z^+ over the Lorentz contracted support of $\Psi(z)$, representing the width of the target (see Refs. [32–34]). Hence, at cross section level, a suppression as $(\gamma_t)^{-1}$ is obtained, corresponding indeed to NEik order.

As a remark, from Eqs. (1) and (2), one obtains as well contributions induced by the instantaneous part of the intermediate quark propagator $S_F(w,z)$ (see Eq. (17) in Ref. [32]). In that case, the photon annihilation and the gluon emission happens simultaneously (meaning $w^+ = z^+$). However, due to the Dirac structure of the instantaneous part of the quark propagator and to the light-cone gauge polarization vectors for QCD and QED, the enhanced components $\Psi^{(-)}(z)$ of the quark background field are projected out, and only the suppressed components $\Psi^{(+)}(z)$ survive. For that reason, the diagrams with simultaneous photon annihilation and gluon emission contribute only at NNEik accuracy at cross section level instead of NEik for the terms calculated in the present paper.

In order to evaluate the "in" contribution, corresponding to Eq. (2) and represented on the right panel of Fig. 1, one needs the quark propagator from the point y inside the target to the point x after the target at eikonal accuracy. It is derived in Ref. [34] and the final result reads

$$S_F(x,y)\big|_{\text{Eik}}^{\text{IA},q} = \int \frac{d^2\mathbf{p}}{(2\pi)^2}\frac{dp^+}{(2\pi)}\frac{\theta(p^+)}{2p^+}e^{-ix\cdot p}(\not{p}+m)$$

$$\times \mathcal{U}_F(x^+,y^+;\mathbf{y})\left[1 - \frac{\gamma^+\gamma^i}{2p^+}i\overleftarrow{\mathcal{D}^F_{\mathbf{y}^i}}\right]e^{iy^-p^+}e^{-i\mathbf{y}\cdot\mathbf{P}}, \qquad (8)$$

where $p^- \equiv (\mathbf{p}^2 + m^2)/(2p^+)$.

The Wilson lines that account for the multiple scattering of the projectile partons off the target gluon field are defined in the standard way as

$$U_R(x^+,y^+;\mathbf{z}) \equiv \mathcal{P}_+ \exp\left\{-ig\int_{y^+}^{x^+} dz^+ T_R \cdot \mathcal{A}^-(z^+,\mathbf{z})\right\}, \qquad (9)$$

where $\mathcal{P}_+$ denotes ordering of color matrices along z^+ direction. The subscript R denotes the representation of the $SU(N)$ generators, either fundamental $(R = F)$ or adjoint $(R = A)$, and $t^a = T_F^a$ and $T^a = T_A^a$. Moreover, we also introduce the following shorthand notation:

$$U_R(\mathbf{z}) \equiv U_R(+\infty, -\infty; \mathbf{z}). \tag{10}$$

The covariant derivatives in representation R are defined as

$$\overrightarrow{\mathcal{D}_{z^\mu}^R} \equiv \overrightarrow{\partial_{z^\mu}} + ig T_R \cdot \mathcal{A}_\mu(z), \tag{11}$$

$$\overleftarrow{\mathcal{D}_{z^\mu}^R} \equiv \overleftarrow{\partial_{z^\mu}} - ig T_R \cdot \mathcal{A}_\mu(z). \tag{12}$$

In a similar way, in order to evaluate the "before" contribution, corresponding to Eq. (1) and represented on the left panel of Fig. 1, one needs the quark propagator from the point y inside the target to the point x before the target and the gluon propagator from the point y inside the target to the point x after the target. These can be calculated at eikonal accuracy [62] and the final results read

$$S_F(x, y)|_{\text{Eik}}^{\text{IB},q} = \int \frac{d^2\mathbf{p}}{(2\pi)^2} \frac{dp^+}{(2\pi)} \frac{\theta(p^+)}{2p^+} e^{ix\cdot p} (\not{p} - m)(-1)$$
$$\times \mathcal{U}_F^\dagger(x^+, y^+; \mathbf{y}) \left[1 + \frac{\gamma^+\gamma^i}{2p^+} i\overleftarrow{\mathcal{D}_{\mathbf{y}^i}^F}\right] e^{-iy^-p^+} e^{i\mathbf{y}\cdot\mathbf{p}} \tag{13}$$

and

$$G_F^{\mu\nu}(x, y)|_{\text{Eik}}^{\text{IA},g} = \int \frac{d^2\mathbf{p}}{(2\pi)^2} \frac{dp^+}{(2\pi)} \frac{\theta(p^+)}{2p^+} e^{-ix\cdot p} \left[-g^{\mu j} + \frac{\mathbf{p}^j}{p^+} g^{\mu+}\right]$$
$$\times \mathcal{U}_A(+\infty, y^+; \mathbf{y}) \left[g_j^\nu + \frac{g^{\nu+}}{p^+}(\mathbf{p}^j + i\overleftarrow{\mathcal{D}_{\mathbf{y}^j}^A})\right]$$
$$\times e^{iy^-p^+} e^{-i\mathbf{y}\cdot\mathbf{p}}. \tag{14}$$

Moreover, we also need the well known expression for the quark eikonal propagator from the point y before the target to the point x after the target which reads

$$S_F(x, y)|_{\text{Eik}}^{\text{BA},q} = \int \frac{d^2\mathbf{p}}{(2\pi)^2} \frac{dp^+}{(2\pi)} \frac{\theta(p^+)}{2p^+} \int \frac{d^2\mathbf{k}}{(2\pi)^2} \frac{dk^+}{(2\pi)} \frac{\theta(k^+)}{2k^+}$$
$$\times e^{-ix\cdot p} e^{iy\cdot k} 2\pi\delta(p^+ - k^+)(\not{p} + m)\gamma^+(\not{k} + m)$$
$$\times \int d^2\mathbf{z} e^{-i\mathbf{z}\cdot(\mathbf{p}-\mathbf{k})} \mathcal{U}_F(+\infty, -\infty; \mathbf{z}). \tag{15}$$

Following the formalism developed in [32–34,62], and using the propagators given in Eqs. (8), (13), and (14),

Eqs. (1) and (2) can be evaluated and lead to the following contributions to the scattering amplitudes[3]

$$i\mathcal{M}_{\gamma_{T,L}\to q_1 g_2}^{\text{bef}} = \frac{iee_f g}{2q^+} \int_{\mathbf{v},\mathbf{z}} e^{-i\mathbf{v}\cdot\mathbf{p}_1 - i\mathbf{z}\cdot\mathbf{p}_2}$$
$$\times \int \frac{d^2\mathbf{K}}{(2\pi)^2} \frac{e^{i(\mathbf{v}-\mathbf{z})\cdot\mathbf{K}}}{[\mathbf{K}^2 + m^2 + \frac{p_1^+ p_2^+}{(q^+)^2}Q^2]}$$
$$\times \overline{u}(1)\frac{\gamma^+\gamma^-}{2}\Gamma_{T,L}^{\text{bef}}\int_{z^+} U_A(+\infty, z^+; \mathbf{z})_{a_2 b}$$
$$\times U_F(\mathbf{v})U_F^\dagger(z^+, -\infty; \mathbf{z})t^b\Psi(z^+, \mathbf{z}), \tag{16}$$

$$i\mathcal{M}_{\gamma_T\to q_1 g_2}^{\text{in}} = \frac{iee_f g}{2q^+} \frac{1}{\left[\left(\mathbf{p}_1 - \frac{p_1^+}{p_2^+}\mathbf{p}_2\right)^2 + m^2\right]}$$
$$\times \int_{\mathbf{z}} e^{-i\mathbf{z}\cdot(\mathbf{p}_1+\mathbf{p}_2)}\overline{u}(1)\frac{\gamma^+\gamma^-}{2}\Gamma_T^{\text{in}}$$
$$\times \int_{z^+} t^{a_2} U_F(+\infty, z^+; \mathbf{z})\Psi(z^+, \mathbf{z}), \tag{17}$$

with

$$\Gamma_L^{\text{bef}} = 2\frac{p_1^+ p_2^+}{(q^+)^2} Q\epsilon_{\lambda_2}^{j*}\gamma^j,$$

$$\Gamma_T^{\text{bef}} = \epsilon_\lambda^i \epsilon_{\lambda_2}^{j*}\left\{\mathbf{K}^l\left[\left(\frac{p_1^+ - p_2^+}{q^+}\right)\delta^{il} - \frac{[\gamma^i, \gamma^l]}{2}\right] + m\gamma^i\right\}\gamma^j, \tag{18}$$

$$\Gamma_T^{\text{in}} = \epsilon_{\lambda_2}^{l*}\epsilon_\lambda^j\left\{\left[\mathbf{p}_1^i - \frac{p_1^+}{p_2^+}\mathbf{p}_2^i\right]\left[-\left(\frac{2p_1^+ + p_2^+}{p_2^+}\right)\delta^{il} + \frac{[\gamma^i, \gamma^l]}{2}\right]\right.$$
$$\left. + m\gamma^l\right\}\gamma^j. \tag{19}$$

III. PRODUCTION CROSS SECTION IN GENERAL DIJET KINEMATICS

The quark-gluon dijet production cross section in DIS for the longitudinal photon case at next-to-eikonal accuracy can be written in general dijet kinematics (without assuming the correlation limit) as

$$(2\pi)^6 (2p_1^+)(2p_2^+)\frac{d\sigma^{\gamma_L\to q_1 g_2}}{dp_1^+ d^2\mathbf{p}_1 dp_2^+ d^2\mathbf{p}_2}$$
$$= (2q^+)(2\pi)\delta(p_1^+ + p_2^+ - q^+)\sum_{h_1,\lambda_2}\sum_{\text{col}} |\mathcal{M}_{\gamma_L\to q_1 g_2}^{\text{bef}}|^2. \tag{20}$$

Using Eq. (16), one gets

---

[3]In the case of longitudinal polarization of the photon, the contribution with photon splitting inside the target (2) is found to vanish at NEik accuracy. Indeed, in light-cone gauge, $\not{\epsilon}_L(q)\Psi(z) = (Q/q^+)\gamma^+\Psi(z)$, and the γ^+ projects the quark field onto its subleading components, see Eq. (5).

$$\sum_{h_1,\lambda_2}\sum_{\text{col}}|\mathcal{M}^{\text{bef}}_{\gamma_L\to q_1g_2}|^2 = \frac{e_f^2\alpha_{\text{em}}\alpha_s}{(2q^+)}16Q^2z^3(1-z)^2\int_{\mathbf{b},\mathbf{b}',\mathbf{r},\mathbf{r}'}e^{-i\mathbf{k}\cdot(\mathbf{b}-\mathbf{b}')}e^{i\mathbf{P}\cdot(\mathbf{r}-\mathbf{r}')}K_0(|\mathbf{r}|\bar{Q})K_0(|\mathbf{r}'|\bar{Q})\int_{z^+,z'^+}$$

$$\times\langle[t^{b'}\mathcal{U}_F(z'^+,-\infty;\mathbf{b}'+z\mathbf{r}')\mathcal{U}_F^\dagger(\mathbf{b}'-(1-z)\mathbf{r}')\mathcal{U}_F(\mathbf{b}-(1-z)\mathbf{r})\mathcal{U}_F^\dagger(z^+,-\infty;b+z\mathbf{r})t^b]_{\beta'\beta}$$

$$\times[\mathcal{U}_A^\dagger(+\infty,z'^+;\mathbf{b}'+z\mathbf{r}')\mathcal{U}_A(+\infty,z^+;\mathbf{b}+z\mathbf{r})]_{b'b}\bar{\Psi}_{\beta'}(z'^+,\mathbf{b}'+z\mathbf{r}')\gamma^-\Psi_\beta(z^+,\mathbf{b}+z\mathbf{r})\rangle. \tag{21}$$

The quark-gluon dijet production cross section in DIS for the transverse photon case at next-to-eikonal accuracy can be written as

$$(2\pi)^6(2p_1^+)(2p_2^+)\frac{d\sigma^{\gamma_T\to q_1g_2}}{dp_1^+d^2\mathbf{p}_1dp_2^+d^2\mathbf{p}_2} = 2q^+(2\pi)\delta(p_1^++p_2^+-q^+)\frac{1}{2}\sum_{\lambda,\lambda_2h_1}\sum_{\text{col}}|\mathcal{M}^{\text{bef}}_{\gamma_T\to q_1g_2}+\mathcal{M}^{\text{in}}_{\gamma_T\to q_1g_2}|^2. \tag{22}$$

Using Eqs. (16) and (17), one obtains

$$\frac{1}{2}\sum_{\lambda,\lambda_2h_1}\sum_{\text{col}}|\mathcal{M}^{\text{in}}_{\gamma_T\to q_1g_2}|^2 = \frac{e_f^2\alpha_{\text{em}}\alpha_sC_F}{[\mathbf{P}^2+(1-z)^2m^2]^2}\frac{(4\pi)^2}{2q^+}z[(1+z^2)\mathbf{P}^2+(1-z)^4m^2]\int d^2\mathbf{z}\int d^2\mathbf{z}'e^{-i\mathbf{k}\cdot(\mathbf{z}-\mathbf{z}')}$$

$$\times\int_{z^+,z'^+}\langle\bar{\Psi}(z'^+,\mathbf{z})\gamma^-\mathcal{U}_F^\dagger(+\infty,z'^+;\mathbf{z}')\mathcal{U}_F(+\infty,z^+;\mathbf{z})\Psi(z^+,\mathbf{z})\rangle, \tag{23}$$

$$\frac{1}{2}\sum_{\lambda,\lambda_2h_1}\sum_{\text{col}}|\mathcal{M}^{\text{bef}}_{\gamma_T\to q_1g_2}|^2 = \frac{e_f^2\alpha_{\text{em}}\alpha_s4z}{(2q^+)}\int_{\mathbf{b},\mathbf{b}',\mathbf{r},\mathbf{r}'}e^{-i\mathbf{k}\cdot(\mathbf{b}-\mathbf{b}')}e^{i\mathbf{P}\cdot(\mathbf{r}-\mathbf{r}')}\int_{b^+,b'^+}\langle[\mathcal{U}_A^\dagger(+\infty,b'^+;\mathbf{b}'+z\mathbf{r}')\mathcal{U}_A(+\infty,b^+;\mathbf{b}+z\mathbf{r})]_{b'b}$$

$$\times[\bar{\Psi}(b'^+,\mathbf{b}'+z\mathbf{r}')t^{b'}\mathcal{U}_F(b'^+,-\infty;\mathbf{b}'+z\mathbf{r}')\mathcal{U}_F^\dagger(\mathbf{b}'-(1-z)\mathbf{r}')]$$

$$\times\gamma^-\left\{[z^2+(1-z)^2]\frac{\mathbf{r}\cdot\mathbf{r}'}{|\mathbf{r}||\mathbf{r}'|}\bar{Q}^2K_1(|\mathbf{r}|\bar{Q})K_1(|\mathbf{r}'|\bar{Q})+m^2K_0(|\mathbf{r}|\bar{Q})K_0(|\mathbf{r}'|\bar{Q})\right.$$

$$\left.+(1-2z)\bar{Q}^2K_1(|\mathbf{r}|\bar{Q})K_1(|\mathbf{r}'|\bar{Q})\frac{\mathbf{r}^l}{|\mathbf{r}|}\frac{\mathbf{r}'^{l'}}{|\mathbf{r}'|}\frac{[\gamma^l,\gamma^{l'}]}{2}\right\}[\mathcal{U}_F(\mathbf{b}-(1-z)\mathbf{r})\mathcal{U}_F^\dagger$$

$$\times(b^+,-\infty;\mathbf{b}+z\mathbf{r})t^b\Psi(b^+,\mathbf{b}+z\mathbf{r})]\rangle, \tag{24}$$

and

$$2\text{Re}\frac{1}{2}\sum_{\lambda,\lambda_2h_1}\sum_{\text{col}}(\mathcal{M}^{\text{in}\dagger}_{\gamma_T\to q_1g_2}\mathcal{M}^{\text{bef}}_{\gamma_T\to q_1g_2}) = -\frac{e_f^2\alpha_{\text{em}}\alpha_s4z}{[\mathbf{P}^2+(1-z)^2m^2]}\frac{(2\pi)}{(2q^+)}2\text{Re}\int_{\mathbf{b},\mathbf{b}',\mathbf{r}}e^{i\mathbf{k}\cdot(\mathbf{b}-\mathbf{b}')}e^{i\mathbf{r}\cdot\mathbf{P}}\int_{b^+,b'^+}$$

$$\times\left\langle[\bar{\Psi}(b'^+,\mathbf{b}')\gamma^-\mathcal{U}_F^\dagger(+\infty,b'^+,\mathbf{b}')t^{a_2}]\left[iz\mathbf{P}^{l'}\frac{\mathbf{r}^l}{|\mathbf{r}|}\bar{Q}K_1(|\mathbf{r}|\bar{Q})\gamma^l\gamma^{l'}+zmK_0(|\mathbf{r}|\bar{Q})\mathbf{P}^l\gamma^l\right.\right.$$

$$\left.+i(1-z)^3m\frac{\mathbf{r}^l}{|\mathbf{r}|}\bar{Q}K_1(|\mathbf{r}|\bar{Q})\gamma^l\right]\mathcal{U}_A(+\infty,b^+;\mathbf{b}+z\mathbf{r})_{a_2b}[\mathcal{U}_F(\mathbf{b}-(1-z)\mathbf{r})$$

$$\left.\times\mathcal{U}_F^\dagger(b^+,-\infty;\mathbf{b}+z\mathbf{r})t^b\Psi(b^+,\mathbf{b}+z\mathbf{r})]\right\rangle, \tag{25}$$

where $K_\alpha(z)$ is the modified Bessel function of the second kind and we used the notation $\bar{Q}^2 = m^2+z(1-z)Q^2$. Moreover, the notation $\langle\cdots\rangle$ stands for target averaging in the spirit of CGC formalism.

IV. PRODUCTION CROSS SECTION IN THE CORRELATION LIMIT

The correlation limit, in which earlier studies have recovered the gluon TMDs from eikonal CGC calculations of $q\bar{q}$ dijets, corresponds to the limit of quasi back-to-back jets [5]. That limit is conveniently expressed in terms of the dijet momentum imbalance $\mathbf{k}$ and relative momentum $\mathbf{P}$, instead of the momenta $\mathbf{p}_1$ and $\mathbf{p}_2$ of the jets, which are defined as

$$\mathbf{P} = (1-z)\mathbf{p}_1-z\mathbf{p}_2, \qquad \mathbf{k} = \mathbf{p}_1+\mathbf{p}_2, \tag{26}$$

with the lightcone momentum fraction $z = p_1^+/(p_1^++p_2^+)$, so that $(1-z) = p_2^+/(p_1^++p_2^+)$. In particular, one has

$$\mathbf{p}_1^i - \frac{p_1^+}{p_2^+}\mathbf{p}_2^i = \frac{\mathbf{P}^i}{(1-z)}. \tag{27}$$

Then, Eq. (17) reads

$$
i\mathcal{M}_{\gamma_T \to q_1 g_2}^{\text{in}} = \frac{iee_f g}{2q^+} \frac{(1-z)^2}{[\mathbf{P}^2 + (1-z)^2 m^2]} \bar{u}(1)\frac{\gamma^+\gamma^-}{2}\Gamma_T^{\text{in}}
$$
$$
\times \int_{\mathbf{b}} e^{-i\mathbf{b}\cdot\mathbf{k}} \int_{z^+} t^{a_2} U_F(+\infty, z^+; \mathbf{b})\Psi(z^+, \mathbf{b}),
\tag{28}
$$

renaming $\mathbf{z}$ into $\mathbf{b}$. The phase factor appearing in the before contribution (16) to the S-matrix becomes

$$e^{-i\mathbf{v}\cdot\mathbf{p}_1 - i\mathbf{z}\cdot\mathbf{p}_2 + i(\mathbf{v}-\mathbf{z})\cdot\mathbf{K}} \to e^{-i\mathbf{k}\cdot\mathbf{b} + i\mathbf{r}\cdot(\mathbf{P}-\mathbf{K})} \tag{29}$$

after defining

$$\mathbf{b} = z\mathbf{v} + (1-z)\mathbf{z}, \qquad \mathbf{r} = \mathbf{z} - \mathbf{v}. \tag{30}$$

The correlation (or back-to-back) limit is defined as $\mathbf{P}^2 \gg \mathbf{k}^2$. Because of the phase factor (29), this implies $\mathbf{r}^2 \ll \mathbf{b}^2$. In that limit, the color structure appearing in Eq. (16) simplifies as

$$
U_A(+\infty, z^+; \mathbf{z})_{a_2 b} U_F(\mathbf{v}) U_F^\dagger(z^+, -\infty; \mathbf{z}) t^b \Psi(z^+, \mathbf{z})
$$
$$
\to U_A(+\infty, z^+; \mathbf{b})_{a_2 b} U_F(\mathbf{b}) U_F^\dagger(z^+, -\infty; \mathbf{b}) t^b \Psi(z^+, \mathbf{b})
$$
$$
= t^{a_2} U_F(+\infty, z^+; \mathbf{b})\Psi(z^+, \mathbf{b}). \tag{31}
$$

Using the approximation (31), the integration over $\mathbf{r}$ can be performed trivially and sets $\mathbf{K} = \mathbf{P}$. All in all, the before contribution (16) to the scattering amplitude reduces to

$$
i\mathcal{M}_{\gamma_{T,L} \to q_1 g_2}^{\text{bef}} \simeq \frac{iee_f g}{2q^+} \frac{1}{[\mathbf{P}^2 + \bar{Q}^2]}\bar{u}(1)\frac{\gamma^+\gamma^-}{2}\Gamma_{T,L}^{\text{bef}}\int_{\mathbf{b}} e^{-i\mathbf{b}\cdot\mathbf{k}}
$$
$$
\times \int_{z^+} t^{a_2} U_F(+\infty, z^+; \mathbf{b})\Psi(z^+, \mathbf{b}) \tag{32}
$$

in the correlation limit $\mathbf{P}^2 \gg \mathbf{k}^2$. Note that Eqs. (28) and (32) contain the same $\mathbf{P}$-independent color structure, and differ only by a $\mathbf{P}$-dependent kinematical factor.

The quark-gluon dijet production cross sections are defined in Eqs. (20) and (22). Evaluating the cross sections in the correlation limit by using the expressions for the scattering amplitudes given in Eqs. (28) and (32), one finds an expression of the form

$$
(2\pi)^6 (2p_1^+)(2p_2^+)\frac{d\sigma^{\gamma_{T,L} \to q_1 g_2}}{dp_1^+ d^2\mathbf{p}_1 dp_2^+ d^2\mathbf{p}_2}\bigg|_{\text{corr lim}}
$$
$$
= 2\pi\delta(p_1^+ + p_2^+ - q^+)(4\pi)^2 \alpha_{\text{em}}\alpha_s C_F e_f^2 \mathcal{H}_{T,L}
$$
$$
\times (\mathbf{P}, z, Q)\mathcal{T}(\mathbf{k}), \tag{33}
$$

where the hard factors for the longitudinal and the transverse photon polarizations are[4]

$$\mathcal{H}_L = \frac{4Q^2 z^3 (1-z)^2}{[\mathbf{P}^2 + \bar{Q}^2]^2}, \tag{34}$$

$$
\mathcal{H}_T = z\left\{\frac{(1+z^2)\mathbf{P}^2 + (1-z)^4 m^2}{[\mathbf{P}^2 + (1-z)^2 m^2]^2} + \frac{[z^2 + (1-z)^2]\mathbf{P}^2 + m^2}{[\mathbf{P}^2 + \bar{Q}^2]^2}\right.
$$
$$
\left. - \frac{2z^2\mathbf{P}^2}{[\mathbf{P}^2 + \bar{Q}^2][\mathbf{P}^2 + (1-z)^2 m^2]}\right\}. \tag{35}
$$

The target-averaged color operator $\mathcal{T}(\mathbf{k})$ reads

$$
\mathcal{T}(\mathbf{k}) = \int_{\mathbf{b}, \mathbf{b}'} e^{-i\mathbf{k}\cdot(\mathbf{b} - \mathbf{b}')}\int_{z^+, z'^+} \langle \bar{\Psi}(z'^+, \mathbf{b}')\gamma^- U_F^\dagger
$$
$$
\times (+\infty, z'^+; \mathbf{b}')U_F(+\infty, z^+; \mathbf{b})\Psi(z^+, \mathbf{b})\rangle. \tag{36}
$$

In general, following the spirit of the CGC formalism, we have calculated the considered scattering process on a semi-classical background field representing the target, and the physical cross section is then obtained after averaging over the target background field, with a suitable probability distribution, see Eqs. (33) and (36). In the context of eikonal scattering in the CGC, only the $\mathcal{A}^-$ component of the background is relevant, and the probability distribution is the solution of the JIMWLK evolution with, in the case of a large nucleus, initial conditions given by the MV model. By contrast, in the example considered in this study, beyond eikonal accuracy, the quark background field of the target is crucial. Two options are in principle possible. Either one could try to generalize the CGC target average, by including the quark background field as well. But no such model is available at the moment. Or one can go back to the quantum expectation value that the CGC target average is supposed to emulate. This is the approach used in this study.

For a given color operator $\mathcal{O}$, the CGC-like target average $\langle\mathcal{O}\rangle$ should be proportional to the quantum expectation value $\langle P_{\text{tar}}|\hat{\mathcal{O}}|P_{\text{tar}}\rangle$ in the state $|P_{\text{tar}}\rangle$ of the target with momentum P_{tar}^μ. In order to ensure the proper normalization $\langle 1\rangle = 1$ and avoid ill defined expressions, one is led to the relation (see for example Refs. [5,7,20,65])

$$\langle\mathcal{O}\rangle = \lim_{P'_{\text{tar}} \to P_{\text{tar}}} \frac{\langle P'_{\text{tar}}|\hat{\mathcal{O}}|P_{\text{tar}}\rangle}{\langle P'_{\text{tar}}|P_{\text{tar}}\rangle}. \tag{37}$$

---

[4]The hard factors for light dijets have been computed in the standard TMD factorization in Refs. [63,64]. After performing the change $z \leftrightarrow (1-z)$ and setting $m = 0$ in Eqs. (34) and (35), and noting that the different definitions of the relative transverse momentum $\mathbf{P}$ here and in [63,64] coincide at leading power accuracy in the correlations limit $\mathbf{P}^2 \gg \mathbf{k}^2$, one can show that the hard factors, $\mathcal{H}_L$ and $\mathcal{H}_T$, computed here match the corresponding hard factors computed in Refs. [63,64].

We choose target states normalized as

$$\langle P'_{\text{tar}}|P_{\text{tar}}\rangle = 2P^-_{\text{tar}}(2\pi)^3\delta(P'^-_{\text{tar}} - P^-_{\text{tar}})\delta^{(2)}(\mathbf{P}'_{\text{tar}} - \mathbf{P}_{\text{tar}}),$$
(38)

following the usual conventions from light-front quantization.[5] In general, in quantum field theory, the translation of any local operator $\hat{\mathcal{O}}(x)$ is obtained by the action of the momentum operator $\hat{P}_\mu$ as

$$\hat{\mathcal{O}}(x) = e^{ia^\mu\hat{P}_\mu}\hat{\mathcal{O}}(x - a)e^{-ia^\mu\hat{P}_\mu}.$$
(39)

Hence, the matrix elements of nonlocal operators behave as

$$\langle P'_{\text{tar}}|\hat{\mathcal{O}}_1(x_1)\cdots\hat{\mathcal{O}}_n(x_n)|P_{\text{tar}}\rangle$$
$$= \langle P'_{\text{tar}}|e^{ia^\mu\hat{P}_\mu}\hat{\mathcal{O}}_1(x_1 - a)\cdots\hat{\mathcal{O}}_n(x_n - a)e^{-ia^\mu\hat{P}_\mu}|P_{\text{tar}}\rangle$$
$$= e^{ia^\mu[(P'_{\text{tar}})_\mu - (P_{\text{tar}})_\mu]}\langle P'_{\text{tar}}|\hat{\mathcal{O}}_1(x_1 - a)\cdots\hat{\mathcal{O}}_n(x_n - a)|P_{\text{tar}}\rangle$$
(40)

under global translations.

Using the relations (37), (38), and (40), one can calculate target-averaged color operator $\mathcal{T}(\mathbf{k})$ from Eq. (36) as

$$\mathcal{T}(\mathbf{k}) = \lim_{P'_{\text{tar}}\to P_{\text{tar}}}\int_{\mathbf{b},\mathbf{b}'}\frac{e^{-i\mathbf{k}\cdot(\mathbf{b}-\mathbf{b}')}}{\langle P'_{\text{tar}}|P_{\text{tar}}\rangle}\int_{z^+,z'^+}\langle P'_{\text{tar}}|\bar{\Psi}(z'^+,\mathbf{b}')\gamma^- U_F^\dagger(+\infty, z'^+; \mathbf{b}')U_F(+\infty, z^+; \mathbf{b})\Psi(z^+, \mathbf{b})|P_{\text{tar}}\rangle$$

$$= \lim_{P'_{\text{tar}}\to P_{\text{tar}}}\int_{\mathbf{b},\mathbf{b}'}\frac{e^{-i\mathbf{k}\cdot(\mathbf{b}-\mathbf{b}')}}{\langle P'_{\text{tar}}|P_{\text{tar}}\rangle}\int_{z^+,z'^+}e^{iz^+(P'^-_{\text{tar}}-P^-_{\text{tar}})}e^{-i\mathbf{b}\cdot(\mathbf{P}'_{\text{tar}}-\mathbf{P}_{\text{tar}})}$$
$$\times \langle P'_{\text{tar}}|\bar{\Psi}(z'^+ - z^+, \mathbf{b}' - \mathbf{b})\gamma^- U_F^\dagger(+\infty, z'^+ - z^+; \mathbf{b}' - \mathbf{b})U_F(+\infty, 0; \mathbf{0})\Psi(0, \mathbf{0})|P_{\text{tar}}\rangle$$

$$= \lim_{P'_{\text{tar}}\to P_{\text{tar}}}\int_{\Delta\mathbf{b}}\frac{e^{i\mathbf{k}\cdot\Delta\mathbf{b}}}{2P^-_{\text{tar}}}\int_{\Delta z^+}\langle P'_{\text{tar}}|\bar{\Psi}(\Delta z^+, \Delta\mathbf{b})\gamma^- U_F^\dagger(+\infty, \Delta z^+; \Delta\mathbf{b})U_F(+\infty, 0; \mathbf{0})\Psi(0, \mathbf{0})|P_{\text{tar}}\rangle,$$
(41)

in which the limit $P'_{\text{tar}} \to P_{\text{tar}}$ can now be taken safely.

The unpolarized TMD quark distribution is defined (up to UV and rapidity regularization issues) as

$$f_1^q(\mathbf{x}, \mathbf{k}) = \frac{1}{(2\pi)^3}\int_{\mathbf{b}}e^{i\mathbf{k}\cdot\mathbf{b}}\int_{z^+}e^{-iz^+\mathbf{x}P^-_{\text{tar}}}\langle P_{\text{tar}}|\bar{\Psi}(z^+, \mathbf{b})\frac{\gamma^-}{2}U_F^\dagger$$
$$\times (+\infty, z^+; \mathbf{b})U_F(+\infty, 0; \mathbf{0})\Psi(0, \mathbf{0})|P_{\text{tar}}\rangle,$$
(42)

where we have neglected the transverse gauge link at infinity. Comparing Eqs. (41) and (42), one finds the relation

$$\mathcal{T}(\mathbf{k}) = \frac{(2\pi)^3}{P^-_{\text{tar}}}f_1^q(\mathbf{x} = 0, \mathbf{k}).$$
(43)

Hence, the differential cross section (33) in the correlation limit becomes a factorization formula involving the quark TMD distribution at $\mathbf{x} = 0$ target momentum fraction:

$$p_1^+ p_2^+ \frac{d\sigma^{\gamma_{T,L}\to q_1 g_2}}{dp_1^+ d^2\mathbf{p}_1 dp_2^+ d^2\mathbf{p}_2}\bigg|_{\text{corr lim}}$$
$$= (2q^+)\delta(p_1^+ + p_2^+ - q^+)\frac{\alpha_{\text{em}}\alpha_s C_F e_f^2}{W^2}$$
$$\times \mathcal{H}_{T,L}(\mathbf{P}, z, Q)f_1^q(\mathbf{x} = 0, \mathbf{k}).$$
(44)

Note that in the denominator of Eq. (44) we have made the high-energy approximation $W^2 = (q + P_{\text{tar}})^2 \simeq 2q^+ P^-_{\text{tar}}$ with W being the center of mass energy of the photon-target collision. This suppression of Eq. (44) as $1/W^2$ at high energy is characteristic of a next-to-eikonal contribution, and here it is due to the exchange of quarks in the t-channel instead of only gluons.

Alternatively, in the correlation limit we can write the cross section in terms of $\mathbf{k}$, z and the dijet mass M_{jj} defined as $M_{jj}^2 \equiv (p_1 + p_2)^2 = \mathbf{P}^2/(z(1-z)) + m^2/z$, and obtain

$$\frac{d\sigma^{\gamma_{T,L}\to q_1 g_2}}{dz dM_{jj}^2 d^2\mathbf{k}}\bigg|_{\text{corr lim}} = (2\pi)\frac{\alpha_{\text{em}}\alpha_s C_F e_f^2}{W^2}\tilde{\mathcal{H}}_{T,L}(M_{jj}, z, Q)$$
$$\times f_1^q(\mathbf{x} = 0, \mathbf{k}),$$
(45)

with the new hard factors

$$\tilde{\mathcal{H}}_L(M_{jj}, z, Q) = \frac{4Q^2 z(1-z)^2}{[(1-z)(M_{jj}^2 + Q^2) + m^2]^2},$$
(46)

___

[5]Note that the formalism that we adopt in this paper corresponds to CGC only in a broad sense. More precisely, it corresponds to the background field method in the high-energy limit. However, we do not rely on semiclassical approximation which is crucial for the CGC effective theory in the strict sense. Equation (37) is then the relation between the quantities calculated in the background field method and their counter parts in the full quantum field theory.

Hard factors (GeV^{-2}), z=0.5, Q=5 GeV

Hard factors (GeV^{-2}), M_{jj}=20 GeV, Q=5 GeV

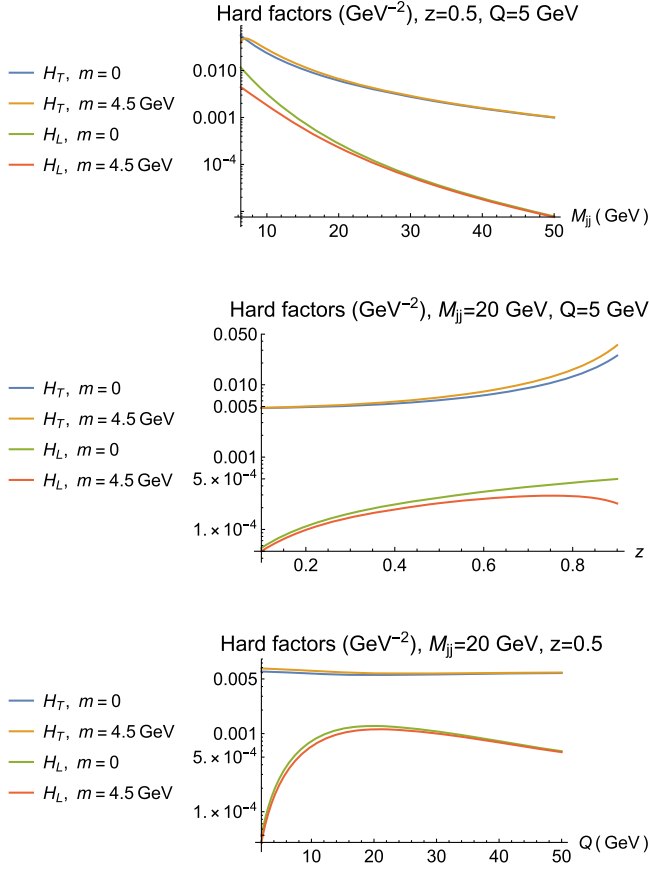Hard factors (GeV^{-2}), M_{jj}=20 GeV, z=0.5

FIG. 2. Hard factors, (46) and (47), versus M_{jj} (top), z (middle, for values such that $|\mathbf{P}| > 6$ GeV) and Q (bottom), for massless and massive ($m = 4.5$ GeV) quarks.

$$\tilde{\mathcal{H}}_T(M_{jj}, z, Q)$$

$$= \frac{(1+z^2)}{(1-z)} \frac{1}{[M_{jj}^2 - m^2]} + \frac{(1-2z)}{[(1-z)(M_{jj}^2 + Q^2) + m^2]}$$

$$+ \frac{(1-z)[2m^2 - (z^2 + (1-z)^2)Q^2]}{[(1-z)(M_{jj}^2 + Q^2) + m^2]^2} - \frac{2m^2}{[M_{jj}^2 - m^2]^2}$$

$$+ \frac{2z(1-z)m^2}{[M_{jj}^2 - m^2][(1-z)(M_{jj}^2 + Q^2) + m^2]}, \tag{47}$$

illustrated on Fig. 2 for massless and bottom quarks. For the chosen values of the variables, $\tilde{\mathcal{H}}_T$ is much larger than $\tilde{\mathcal{H}}_L$, hard factors decrease with M_{jj}, and $\tilde{\mathcal{H}}_T$ is notably flat with Q. Overall, the influence of the quark mass m is moderate, except in the small M_{jj} region close to the kinematical limit, and for $z \to 1$. However, these two limits are outside of the validity region of our approach.

V. DISCUSSION

In this paper we have studied the process of quark-gluon dijet production in DIS at high energy in the CGC. Such process is mediated by a quark exchange in the t-channel

and thus it is subeikonal. Going to the correlation limit of almost back-to-back jets, we have established the relation with the unpolarized quark TMD distribution at small x.

At this stage, we would like to comment on the difference between the quark TMD appearing in our results and the one appearing in Ref. [13]. In the present manuscript, the operator definition of the quark TMD (up to regularization issues) is obtained from the analysis of the cross section and therefore it is the full quark TMD distribution containing both sea and valence contributions. By contrast, in Ref. [13], the authors calculate SIDIS in the dipole approach, in pure gluon background field, and interpret part of their result as the sea contribution to the quark TMD. This is analog to write, in the collinear factorization, the sea contribution to the quark PDF as the gluon PDF convoluted with a coefficient accounting for a gluon to quark extra step of DGLAP evolution.

The determination of the quark TMD distributions proposed here relies on the identification of quark-gluon jets in DIS. In the case of light quarks, such identification is challenging, see, e.g., [66,67] and references therein. However, machine learning techniques might improve the discrimination of light quarks and gluon jets in the future [68].

Another possibility would be considering heavy flavor jets, whose discrimination from light quark or gluon jets is better established. The expressions provided in this paper consider quark masses so they can be applied for heavy flavors. Of course, that would restrict the study to heavy flavor TMD distributions in the target.

On the other hand, the process studied here competes with the eikonal production of a quark, an antiquark and a gluon at partonic level, where the quark and gluon fragment into separate jets and the antiquark does not belong to these two tagged jets. Even though this process is of higher order in α_s compared to the mechanism studied in this manuscript, in the high energy limit it is enhanced since it is an eikonal contribution and not a next-to-eikonal one. A proper comparison of both mechanisms in the EIC kinematics requires a dedicated effort and it is beyond the scope of this work. Nevertheless, it is expected that the contamination by this background mechanism can be significantly reduced by imposing appropriate experimental cuts.

Indeed, in this background mechanism, the antiquark is typically carrying away sizable longitudinal and transverse momenta. The contribution (45) obeys $p_1^+ + p_2^+ = q^+$ exactly, whereas the background contribution obeys $0 < p_1^+ + p_2^+ < q^+$, with no expected enhancement for $p_1^+ + p_2^+ \to q^+$. Hence, experimentally, one can impose that the total lightcone momentum of the dijet $p_1^+ + p_2^+$ is close enough to the incoming photon momentum q^+ in order to significantly reduce the background contribution. Similarly, in the background contribution the transverse momentum of the produced antiquark is typically of the same order as the one of the produced quark. For that reason, imposing the back-to-back limit $\mathbf{P}^2 \gg \mathbf{k}^2$ with $\mathbf{P}$

and **k** defined as in Eq. (26) from the quark and gluon jets momenta should further suppress the background contribution. While additional studies are required, we think that with these experimental cuts the process of quark-gluon dijet production in DIS at the EIC is a promising new method to probe the quark TMD distribution in addition to semi-inclusive DIS and Drell-Yan production, see, e.g., [4,69] and references therein.

ACKNOWLEDGMENTS

[1] Y. V. Kovchegov and E. Levin, *Quantum Chromodynamics at High Energy* (Cambridge University Press, Cambridge, England, 2012), Vol. 33.

[2] F. Gelis, E. Iancu, J. Jalilian-Marian, and R. Venugopalan, Annu. Rev. Nucl. Part. Sci. **60**, 463 (2010).

[3] J. Collins, *Foundations of Perturbative QCD* (Cambridge University Press, Cambridge, England, 2013), Vol. 32.

[4] R. Boussarie *et al.*, arXiv:2304.03302.

[5] F. Dominguez, C. Marquet, B.-W. Xiao, and F. Yuan, Phys. Rev. D **83**, 105005 (2011).

[6] F. Dominguez, C. Marquet, A. M. Stasto, and B.-W. Xiao, Phys. Rev. D **87**, 034007 (2013).

[7] C. Marquet, E. Petreska, and C. Roiesnel, J. High Energy Phys. 10 (2016) 065.

[8] E. Petreska, Int. J. Mod. Phys. E **27**, 1830003 (2018).

[9] C. Marquet, C. Roiesnel, and P. Taels, Phys. Rev. D **97**, 014004 (2018).

[10] T. Altinoluk, N. Armesto, A. Kovner, M. Lublinsky, and E. Petreska, J. High Energy Phys. 04 (2018) 063.

[11] T. Altinoluk, R. Boussarie, C. Marquet, and P. Taels, J. High Energy Phys. 07 (2019) 079.

[12] T. Altinoluk, R. Boussarie, C. Marquet, and P. Taels, J. High Energy Phys. 07 (2020) 143.

[13] C. Marquet, B.-W. Xiao, and F. Yuan, Phys. Lett. B **682**, 207 (2009).

[14] Y. Hatta, B.-W. Xiao, and F. Yuan, Phys. Rev. D **106**, 094015 (2022).

[15] P. Taels, T. Altinoluk, G. Beuf, and C. Marquet, J. High Energy Phys. 10 (2022) 184.

[16] P. Caucal, F. Salazar, B. Schenke, and R. Venugopalan, J. High Energy Phys. 11 (2022) 169.

[17] P. Kotko, K. Kutak, C. Marquet, E. Petreska, S. Sapeta, and A. van Hameren, J. High Energy Phys. 09 (2015) 106.

[18] A. van Hameren, P. Kotko, K. Kutak, C. Marquet, E. Petreska, and S. Sapeta, J. High Energy Phys. 12 (2016) 034; 02 (2019) 158(E).

[19] T. Altinoluk, R. Boussarie, and P. Kotko, J. High Energy Phys. 05 (2019) 156.

[20] T. Altinoluk and R. Boussarie, J. High Energy Phys. 10 (2019) 208.

[21] R. Boussarie and Y. Mehtar-Tani, Phys. Rev. D **103**, 094012 (2021).

[22] H. Fujii, C. Marquet, and K. Watanabe, J. High Energy Phys. 12 (2020) 181.

[23] T. Altinoluk, C. Marquet, and P. Taels, J. High Energy Phys. 06 (2021) 085.

[24] R. Boussarie, H. Mäntysaari, F. Salazar, and B. Schenke, J. High Energy Phys. 09 (2021) 178.

[25] T. Altinoluk, N. Armesto, G. Beuf, M. Martínez, and C. A. Salgado, J. High Energy Phys. 07 (2014) 068.

[26] T. Altinoluk, N. Armesto, G. Beuf, and A. Moscoso, J. High Energy Phys. 01 (2016) 114.

[27] T. Altinoluk and A. Dumitru, Phys. Rev. D **94**, 074032 (2016).

[28] P. Agostini, T. Altinoluk, and N. Armesto, Eur. Phys. J. C **79**, 600 (2019).

[29] P. Agostini, T. Altinoluk, and N. Armesto, Eur. Phys. J. C **79**, 790 (2019).

[30] P. Agostini, T. Altinoluk, N. Armesto, F. Dominguez, and J. G. Milhano, Eur. Phys. J. C **82**, 1001 (2022).

[31] P. Agostini, T. Altinoluk, and N. Armesto, Phys. Lett. B **840**, 137892 (2023).

[32] T. Altinoluk, G. Beuf, A. Czajka, and A. Tymowska, Phys. Rev. D **104**, 014019 (2021).

[33] T. Altinoluk and G. Beuf, Phys. Rev. D **105**, 074026 (2022).

[34] T. Altinoluk, G. Beuf, A. Czajka, and A. Tymowska, Phys. Rev. D **107**, 074016 (2023).

[35] Y. V. Kovchegov, D. Pitonyak, and M. D. Sievert, J. High Energy Phys. 01 (2016) 072; 10 (2016) 148(E).

[36] Y. V. Kovchegov, D. Pitonyak, and M. D. Sievert, Phys. Rev. D **95**, 014033 (2017).

[37] Y. V. Kovchegov, D. Pitonyak, and M. D. Sievert, Phys. Rev. Lett. **118**, 052001 (2017).

[38] Y. V. Kovchegov, D. Pitonyak, and M. D. Sievert, Phys. Lett. B **772**, 136 (2017).

[39] Y. V. Kovchegov, D. Pitonyak, and M. D. Sievert, J. High Energy Phys. 10 (2017) 198.

[40] Y. V. Kovchegov and M. D. Sievert, Phys. Rev. D **99**, 054032 (2019).

[41] F. Cougoulic and Y. V. Kovchegov, Phys. Rev. D **100**, 114020 (2019).

[42] Y. V. Kovchegov and Y. Tawabutr, J. High Energy Phys. 08 (2020) 014.

[43] F. Cougoulic and Y. V. Kovchegov, Nucl. Phys. **A1004,** 122051 (2020).

[44] D. Adamiak, Y. V. Kovchegov, W. Melnitchouk, D. Pitonyak, N. Sato, and M. D. Sievert (Jefferson Lab Angular Momentum Collaboration), Phys. Rev. D **104,** L031501 (2021).

[45] Y. V. Kovchegov, A. Tarasov, and Y. Tawabutr, J. High Energy Phys. 03 (2022) 184.

[46] Y. V. Kovchegov and M. G. Santiago, J. High Energy Phys. 11 (2021) 200; 09 (2022) 186(E).

[47] F. Cougoulic, Y. V. Kovchegov, A. Tarasov, and Y. Tawabutr, J. High Energy Phys. 07 (2022) 095.

[48] Y. V. Kovchegov and M. G. Santiago, J. High Energy Phys. 11 (2022) 098.

[49] G. A. Chirilli, J. High Energy Phys. 01 (2019) 118.

[50] G. A. Chirilli, J. High Energy Phys. 06 (2021) 096.

[51] I. Balitsky and A. Tarasov, J. High Energy Phys. 10 (2015) 017.

[52] I. Balitsky and A. Tarasov, J. High Energy Phys. 06 (2016) 164,.

[53] I. Balitsky and A. Tarasov, J. High Energy Phys. 07 (2017) 095.

[54] R. Boussarie and Y. Mehtar-Tani, Phys. Lett. B **831,** 137125 (2022).

[55] R. Boussarie and Y. Mehtar-Tani, J. High Energy Phys. 07 (2022) 080.

[56] J. Jalilian-Marian, Phys. Rev. D **96,** 074020 (2017).

[57] J. Jalilian-Marian, Phys. Rev. D **99,** 014043 (2019).

[58] J. Jalilian-Marian, Phys. Rev. D **102,** 014008 (2020).

[59] A. Accardi et al., Eur. Phys. J. A **52,** 268 (2016).

[60] R. Abdul Khalek et al., Nucl. Phys. **A1026,** 122447 (2022).

[61] N. N. Nikolaev and B. G. Zakharov, Z. Phys. C **49,** 607 (1991).

[62] T. Altinoluk, G. Beuf, and S. Mulani (to be published).

[63] D. Boer, P. J. Mulders, C. Pisano, and J. Zhou, J. High Energy Phys. 08 (2016) 001.

[64] R. F. del Castillo, M. G. Echevarria, Y. Makris, and I. Scimemi, J. High Energy Phys. 03 (2022) 047.

[65] A. V. Belitsky, X. Ji, and F. Yuan, Nucl. Phys. **B656,** 165 (2003).

[66] A. J. Larkoski, I. Moult, and B. Nachman, Phys. Rep. **841,** 1 (2020).

[67] R. Kogler et al., Rev. Mod. Phys. **91,** 045003 (2019).

[68] K. Lee, J. Mulligan, M. Płoskoń, F. Ringer, and F. Yuan, J. High Energy Phys. 03 (2023) 085.

[69] R. Angeles-Martinez et al., Acta Phys. Pol. B **46,** 2501 (2015).